Hierarchic superradiant phases in anisotropic Dicke model

D. K. He, Z. Song*

School of Physics, Nankai University, Tianjin 300071, China

$\star$ songtc@nankai.edu.cn

Abstract

We revisit the phase diagram of an anisotropic Dicke model by revealing the non-analyticity induced by underlying exceptional points. We find that, from a dynamical perspective, the conventional superradiant phase can be further separated into three regions, in which the systems are characterized by different effective Hamiltonians, including the harmonic oscillator, the inverted harmonic oscillator, and their respective counterparts. We employ the Loschmidt echo to characterize different quantum phases by analyzing the quench dynamics of a trivial initial state. Numerical simulations for finite systems confirm our predictions about the existence of hierarchic superradiant phases.

1 Introduction

With the gradual development of experiments on light-matter interaction [1–4], the quantum simulation of the Dicke model [5–8] is transitioning from theory to experiment. The Dicke

model [9–13] is a fundamental model in the field of quantum optics, describing the interaction between a single-mode light field and N two-level atoms. The Dicke model has a broad prospect and great potential in the field of quantum batteries [14–20]. In the thermodynamic limit ($N \rightarrow \infty$), the ground state of the Dicke model undergoes a quantum phase transition (QPT) from the normal phase (NP) to the superradiant phase (SP) [11–13,21–24] at a certain critical coupling strength, which is referred to as the superradiant phase transition. In addition to the QPT of the ground state demonstrated above, the Dicke model also exhibits three distinct phase transitions, namely, the dissipative phase transition (non-equilibrium quantum phase transition) [25–27], the excited-state quantum phase transition [28–30], and the thermal phase transition [31,32].

The concept of exceptional points (EPs) [33–35], which represents the degeneracies of non-Hermitian operators, is regarded as a unique feature of non-Hermitian systems. However, subsequent research has shown that EPs exist not only in non-Hermitian systems but also in Hermitian systems [36–48] . The non-analyticity induced by EPs suggests the presence of a phase transition at this point. In previous studies, we demonstrated that the superradiant quantum phase transition in the Dicke model can be seen as the effect of two hidden second-order EPs [48,49]. This quantum phase transition is a dynamical phase transition, because as the parameter varies, the effective form of the Hamiltonian changes, resulting in completely different dynamical behaviors on either side of the transition point. This drives us to seek a more general Dicke model to investigate its dynamical phase transitions. A more general version of the Dicke model is called the anisotropic Dicke model [20,50–55] (ADM), in which the strengths of the rotating-wave and counter-rotating-wave terms are different. The ADM is being widely studied, including its applications in quantum batteries [20] and the ergodic-to-nonergodic transition [50,51], as well as work related to quantum chaos [53].

In this work, we focus on the ADM Hamiltonian and identify the hidden EPs of this Hamiltonian in the thermodynamic limit. The EPs divide the parameter space into four regions. The results show that, in addition to the existing NP to SP transition, there exists a hierarchical structure within the SP phase. In each region, the original Hamiltonian consists of different combinations of equivalent Hamiltonians, including the harmonic oscillator and the inverted harmonic oscillator [56,57]. The dynamics of such two oscilators are fundamentally different. Therefore, starting from an initial state with only a small atomic excitation, the distinct finite-time dynamical behaviors of the ADM can be used to demonstrate the existence of EPs and to discriminate between different quantum phases. The finite-time guarantee ensures that the dynamics of an ADM with a finite atom number can still be accurately described by the thermodynamic-limit ADM, an idea akin to that proposed in [58]. We employ the Loschmidt echo of quench dynamics to characterize these phase transitions. The Loschmidt echo can be measured experimentally using quantum state tomography [59–61].

The structure of this paper is as follows. In Sec. 2, we introduce the model and pointed out the hidden EPs within it. In Sec. 3, we solve the Hamiltonian exactly and present the phase diagram of the model. In Sec. 4, we utilize quench dynamics to calculate the Loschmidt echo in order to identify different dynamical phases. Finally, in Sec. 5, we provide a summary and discussion. Some details of the calculations are provided in the Appendix.
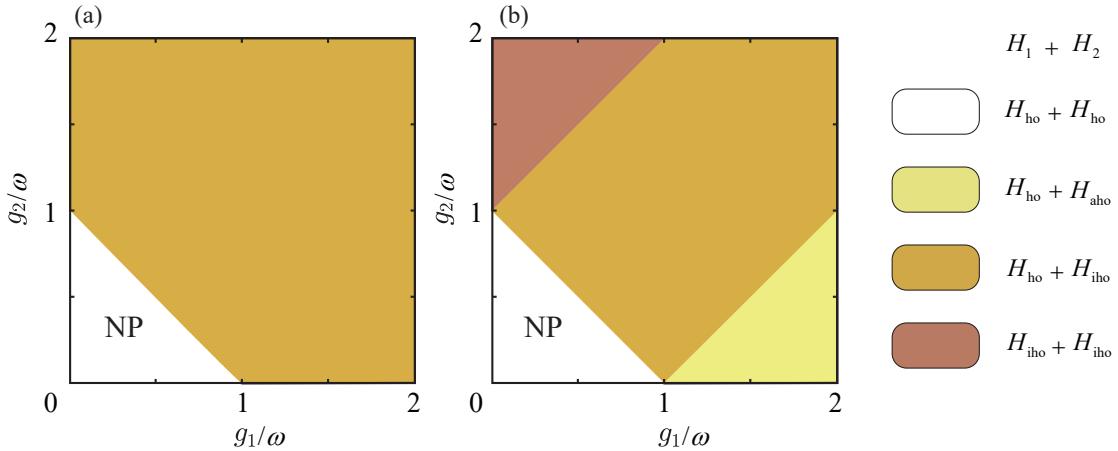
Figure 1: Phase diagrams of the Hamiltonian in Eq. (1) on the parameter $g_1 g_2$ plane, indicating the main conclusion of this work. Different colors in the diagram distinguish different phases of the system. (a) The traditional phase diagram of the anisotropic Dicke model (ADM), obtained by the mean field method, shows that the region $g_1 + g_2 < \omega$ corresponds to the normal phase (NP), and the region $g_1 + g_2 > \omega$ corresponds to the superradiant phase (SP). (b) The phase diagram of the ADM, revealed by the underlying exceptional points (EPs) of the effective Hamiltonian in Eq. (4) of the system, shows that the original superradiant phase (a) can be further divided into three distinct phases. We label these phases as SP_1, SP_2, and SP_3, respectively. The corresponding equivalent Hamiltonians of the effective Hamiltonian in each region are indicated in the panel. Here, we assume $\omega = \omega_0$.

2 Model and exceptional points

We consider a Hamiltonian of a single-mode boson coupled to N two-level atoms, where the rotating-wave and counter-rotating-wave terms are distinct. This model is known as the ADM.

$$
\begin{aligned}
H = {} & \omega a^\dagger a + \omega_0 J_z + \frac{g_1}{\sqrt{N}}\left(a^\dagger J_- + a J_+\right) \\
& + \frac{g_2}{\sqrt{N}}\left(a^\dagger J_+ + a J_-\right).
\end{aligned}
\tag{1}
$$

Here, $a^\dagger$ and a represent the creation and annihilation operators of the single-mode boson, respectively. $J_\pm$ and J_z are the collective atomic operators, and their commutation relations are as follows

$$
\left[a, a^\dagger\right] = 1, [J_z, J_\pm] = \pm J_\pm, [J_+, J_-] = 2J_z.
\tag{2}
$$

The first and second terms of the Hamiltonian represent the free Hamiltonians of the light field and the N two-level atoms, respectively, with their strengths controlled by ω and ω_0. The third and fourth terms correspond to the rotating-wave and counter-rotating-wave coupling terms, with coupling strengths g_1 and g_2, respectively. When $g_1 = g_2$, the model reduces to the Dicke model. For convenience, in the following derivations, we assume $\omega = \omega_0$, $g_1 > 0$, $g_2 > 0$. The phase diagram of the ADM has been conclusively established in previous studies based on the mean field method [51]. In the parameter plane of $g_1 g_2$, the region where $g_1 + g_2 > \omega$ corresponds to the superradiant phase, while the region where $g_1 + g_2 < \omega$ corresponds to the normal phase. Although the standard Dicke model in cavity QED is prohibited from exhibiting the superradiant phase due to the no-go theorem [62, 63], recent studies have shown that anisotropy can overcome the no-go theorem [55, 64], thus providing a theoretical basis for

its potential experimental realization in platforms such as cavity QED. The phase diagram is shown in Fig. 1(a).

In the following, we will show that the conventional superradiant phase can be further separated into three regions, in which the systems are characterized by different effective Hamiltonians in large N limit, including the harmonic oscillator, the inverted harmonic oscillator, and their respective counterparts. We refer to these as hierarchic superradiant phases because the same given initial state exhibits distinct dynamic behaviors.

We introduce the Holstein-Primakoff (HP) transformation to convert the spin operators into bosonic operators b

$$
\begin{aligned}
J_z &= b^\dagger b - \frac{N}{2}, \\
J_+ &= (J_-)^\dagger = b^\dagger \sqrt{N - b^\dagger b},
\end{aligned}
\tag{3}
$$

In the thermodynamic limit where $N \to \infty$ and neglecting constant terms, the Hamiltonian can be rewritten as

$$
\begin{aligned}
H_{\text{eff}} &= \omega\left(a^\dagger a + b^\dagger b\right) + g_1\left(a^\dagger b + a b^\dagger\right) \\
&\quad + g_2\left(a^\dagger b^\dagger + a b\right).
\end{aligned}
\tag{4}
$$

H_{eff} can be regarded as a two-site Hermitian bosonic Kitaev model [48, 49, 65]. In previous studies, we revealed that this model possesses hidden EPs. We introduce a linear transformation

$$
d_{1,2} = \frac{1}{\sqrt{2}}(a \pm b),
\tag{5}
$$

to decompose H_{eff} into two independent subspaces Hamiltonian can be written as

$$
\begin{aligned}
H_{\text{eff}} &= H_1 + H_2 \\
&= \phi_L \begin{pmatrix} h_1 & 0 \\ 0 & h_2 \end{pmatrix} \phi_R.
\end{aligned}
\tag{6}
$$

The non-Hermitian Nambu spinor is defined as $\phi_L = \left(d_1, -d_1^\dagger, d_2, -d_2^\dagger\right)$ and $\phi_R = \left(d_1^\dagger, d_1, d_2^\dagger, d_2\right)^T$. This representation has been studied in Ref. [36–38], and it can be generalized to arbitrary quadratic bosonic systems. The forms of the two matrices are

$$
h_{1,2} = \frac{1}{2}\left(\omega \pm g_1\right)\sigma_z \pm \frac{i}{2}g_2\sigma_y,
\tag{7}
$$

$h_{1,2}$ are non-Hermitian matrices, and σ_z and σ_y are Pauli matrices, defined as

$$
\sigma_z = \begin{pmatrix} 1 & 0 \\ 0 & -1 \end{pmatrix}, \sigma_y = \begin{pmatrix} 0 & -i \\ i & 0 \end{pmatrix}.
\tag{8}
$$

The eigenvalues of $h_{1,2}$ are

$$
\begin{aligned}
\lambda_1^\pm &= \pm\frac{1}{2}\sqrt{(\omega + g_1)^2 - g_2^2}, \\
\lambda_2^\pm &= \pm\frac{1}{2}\sqrt{(\omega - g_1)^2 - g_2^2}.
\end{aligned}
\tag{9}
$$

The corresponding right eigenvectors are

$$
\begin{aligned}
\phi_1^\pm &= \begin{pmatrix} -\frac{1}{g_2}\left(\omega + g_1 + 2\lambda_1^\pm\right) \\ 1 \end{pmatrix}, \\
\phi_2^\pm &= \begin{pmatrix} \frac{1}{g_2}\left(\omega - g_1 + 2\lambda_2^\pm\right) \\ 1 \end{pmatrix}.
\end{aligned}
\tag{10}
$$

From the forms of the eigenvalues and eigenvectors, we can see that the matrices possess EPs. h_1 has a second-order EP when $|\omega + g_1| = |g_2|$, and h_2 has a second-order EP when $|\omega - g_1| = |g_2|$. These EP can divide different regions in the $g_1 - g_2$ parameter plane, as shown in Fig. 1(b). In the next section, we will provide the exact solutions for the diagonalized Hamiltonian in each region.

3   Phase diagram

The Hamiltonians H_1 and H_2 can be explicitly expressed as follows:

$$H_1 = (\omega + g_1) d_1^\dagger d_1 + \frac{g_2}{2} \left(d_1^\dagger d_1^\dagger + d_1 d_1 \right), \tag{11}$$

and

$$H_2 = (\omega - g_1) d_2^\dagger d_2 - \frac{g_2}{2} \left(d_2^\dagger d_2^\dagger + d_2 d_2 \right), \tag{12}$$

respectively. We note that the two Hamiltonians have the same form as

$$\mathcal{H} = \mu \beta^\dagger \beta + \frac{\Delta}{2} \left(\beta^\dagger \beta^\dagger + \beta \beta \right), \tag{13}$$

where β is the bosonic annihilation operator. In the Appendix A, we provide the derivation of the diagonalization of the Hamiltonian $\mathcal{H}$, based on which two Hamiltonians H_1 and H_2 can be reduced to different simple form in the four regions in the first quadrant of $g_1 g_2$ plane.

Ignoring the energy constants, there exist three types of equivalent Hamiltonians, given by

$$H_{\text{ho}} = \Omega_i \left(\gamma_i^\dagger \gamma_i + \frac{1}{2} \right), \tag{14}$$

$$H_{\text{iho}} = (-1)^{i+1} \frac{\Omega_i}{2} \left[\left(\gamma_i^\dagger \right)^2 + \gamma_i^2 \right], \tag{15}$$

$$H_{\text{aho}} = -\Omega_i \left(\gamma_i^\dagger \gamma_i + \frac{1}{2} \right), \tag{16}$$

with $i = 1, 2$, where γ_i are bosonic annihilation operators. The positive factor Ω_i is given by

$$\Omega_1 = \omega \left| \sqrt{\left(1 + \frac{g_1}{\omega} \right)^2 - \left(\frac{g_2}{\omega} \right)^2} \right|, \tag{17}$$

$$\Omega_2 = \omega \left| \sqrt{\left(1 - \frac{g_1}{\omega} \right)^2 - \left(\frac{g_2}{\omega} \right)^2} \right|. \tag{18}$$

The harmonic oscillator Hamiltonian H_{ho} is the standard form of the Hamiltonian for a harmonic oscillator. The inverted harmonic oscillator Hamiltonian H_{iho} describes a system with an inverted potential; its eigenenergies are continuous and unbounded [57], rendering the system unstable and allowing it to tunnel toward states with higher particle numbers [66]. In Appendix B, we present a detailed account of the dynamical characteristics of this Hamiltonian. The anti-harmonic oscillator Hamiltonian H_{aho} is the negative of the standard harmonic oscillator Hamiltonian. For H_2, when $|\omega - g_1| > g_2$ and $\omega - g_1 < 0$, the system diagonalizes into such an anti-harmonic oscillator. The anti-harmonic oscillator describes a system where the vacuum state has the highest energy, and states with higher particle numbers have lower energies. Its dynamics under isolated conditions are oscillatory, just like those of a standard harmonic oscillator. Each of these Hamiltonians has distinct physical properties and implications for the stability and behavior of the system. Under the dynamics of an isolated system,

the harmonic oscillator and anti-harmonic oscillator are stable, while the inverted harmonic oscillator is unstable. In the following, we present the explicit form of the equivalent Hamiltonians in each region.
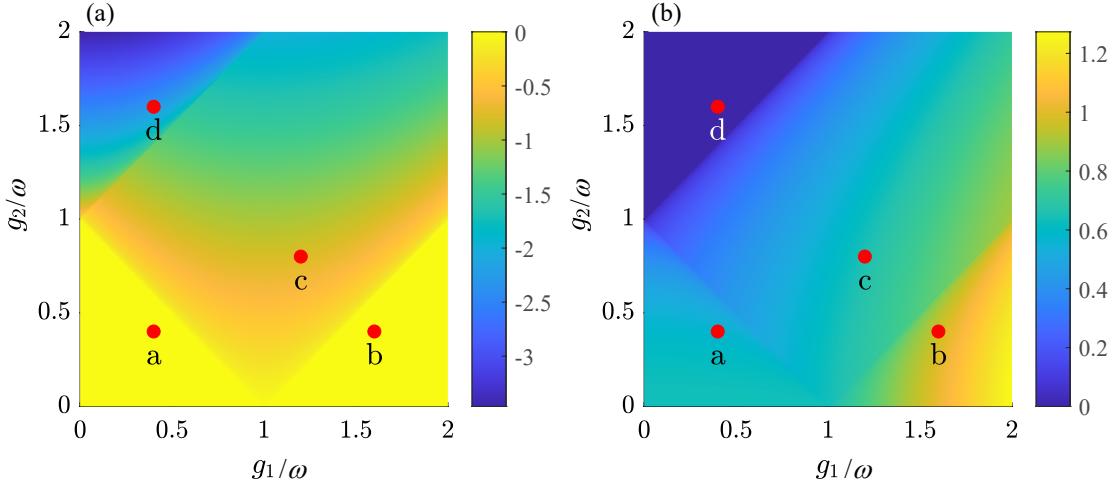
Figure 2: The plots of the decay rate λ in (a), given by Eq. (41) and frequency f in (b), given by Eq. (42) of the effective Hamiltonian on the g_1/ω-g_2/ω plane. It can be seen from the figures that there are clear distinctions between different phases in terms of λ and f. Four representitive points in each regions are selected, indicated by red dots at the same positions in both panels, with coordinates a(0.4, 0.4), b(1.6, 0.4), c(1.2, 0.8), and d(0.4, 1.6). The corresponding quench dynamical behaviors of the original ADM in finite systems at these points, obtained by numerical simulations, are presented in Fig. 3.

(i) For $g_1 + g_2 < \omega$, in this region, the two Hamiltonians have the form

$$H_1 = \Omega_1 \left(\gamma_1^\dagger \gamma_1 + \frac{1}{2} \right) - \frac{1}{2} (\omega + g_1), \tag{19}$$

and

$$H_2 = \Omega_2 \left(\gamma_2^\dagger \gamma_2 + \frac{1}{2} \right) - \frac{1}{2} (\omega - g_1), \tag{20}$$

respectively. Here, γ_1 and γ_2 are bosonic annihilation operators, given by

$$\gamma_i = \sinh(\theta_i) d_i^\dagger + \cosh(\theta_i) d_i, \tag{21}$$

with

$$\tanh(\theta_1) = \frac{\omega + g_1 - \Omega_1}{g_2}, \tag{22}$$

and

$$\tanh(\theta_2) = \frac{\omega - g_1 - \Omega_2}{g_2}, \tag{23}$$

respectively. This part corresponds to the NP region in Fig. 1(b).

(ii) For $g_1 + g_2 > \omega$ and $g_2 < g_1 - \omega$, in this region, two Hamiltonians have the form

$$H_1 = \Omega_1 \left(\gamma_1^\dagger \gamma_1 + \frac{1}{2} \right) - \frac{1}{2} (\omega + g_1), \tag{24}$$

and

$$H_2 = -\Omega_2 \left(\gamma_2^\dagger \gamma_2 + \frac{1}{2} \right) - \frac{1}{2} (\omega - g_1), \tag{25}$$

respectively. Here, γ_1, γ_2, $\tanh(\theta_1)$ and $\tanh(\theta_2)$ have the same forms in Eqs. (21),(22) and (23). This part corresponds to the SP_1 region in Fig. 1(b).

(iii) For $g_1 + g_2 > \omega$ and $g_1 - \omega < g_2 < g_1 + \omega$, in this region, two Hamiltonians have the form

$$H_1 = \Omega_1 \left(\gamma_1^\dagger \gamma_1 + \frac{1}{2} \right) - \frac{1}{2} (\omega + g_1), \tag{26}$$

and

$$H_2 = i \frac{\Omega_2}{2} \left[(\gamma_2^\dagger)^2 + (\gamma_2)^2 \right] - \frac{1}{2} (\omega - g_1), \tag{27}$$

respectively. Here, γ_1 and γ_2 have the same forms in Eq. (21), but with

$$\tanh(\theta_1) = \frac{(\omega + g_1) - \Omega_1}{g_2}, \tag{28}$$

and

$$\tanh(\theta_2) = \frac{g_2 - i\Omega_2}{\omega - g_1}. \tag{29}$$

This part corresponds to the SP_2 region in Fig. 1(b).

(iv) For $g_1 + g_2 > \omega$ and $g_1 + \omega < g_2$, in this region, two Hamiltonians have the form

$$H_1 = -i \frac{\Omega_1}{2} \left[(\gamma_2^\dagger)^2 + (\gamma_2)^2 \right] - \frac{1}{2} (\omega + g_1), \tag{30}$$

and

$$H_2 = i \frac{\Omega_2}{2} \left[(\gamma_2^\dagger)^2 + (\gamma_2)^2 \right] - \frac{1}{2} (\omega - g_1), \tag{31}$$

respectively. Here, γ_1 and γ_2 have the same forms in Eq. (21), but with

$$\tanh(\theta_1) = \frac{g_2 + i\Omega_1}{\omega + g_1}, \tag{32}$$

and

$$\tanh(\theta_2) = \frac{g_2 - i\Omega_2}{\omega - g_1}, \tag{33}$$

respectively. This part corresponds to the SP_3 region in Fig. 1(b). The corresponding equivalent Hamiltonians are indicated in the phase diagram shown in Fig. 1(b). It shows that the configurations of the equivalent Hamiltonians are different in each region. The whole superradiant phase is separated three sub-phases, which are refered to as hierarchic superradiant phases. Here, we would like to emphasize that the phase diagram presented here is not a zero-temperature phase diagram. Different equivalent Hamiltonians exhibit different dynamics, which cannot be captured by mean-field theory. These phases have to be detected by the measurement of information in the excited state. Building upon this insight, we will propose a dynamic demonstration of the phase diagram.

4   Quench dynamics

In this section, we investigate the dynamic behavior of the phase diagram, including the hierarchical superradiant phases. We consider the quench dynamics under the postquench Hamiltonian H. We conduct numerical simulations for the Loschmidt echo, defined as

$$L(t) = |\langle \psi(0) | \psi(t) \rangle|^2, \tag{34}$$
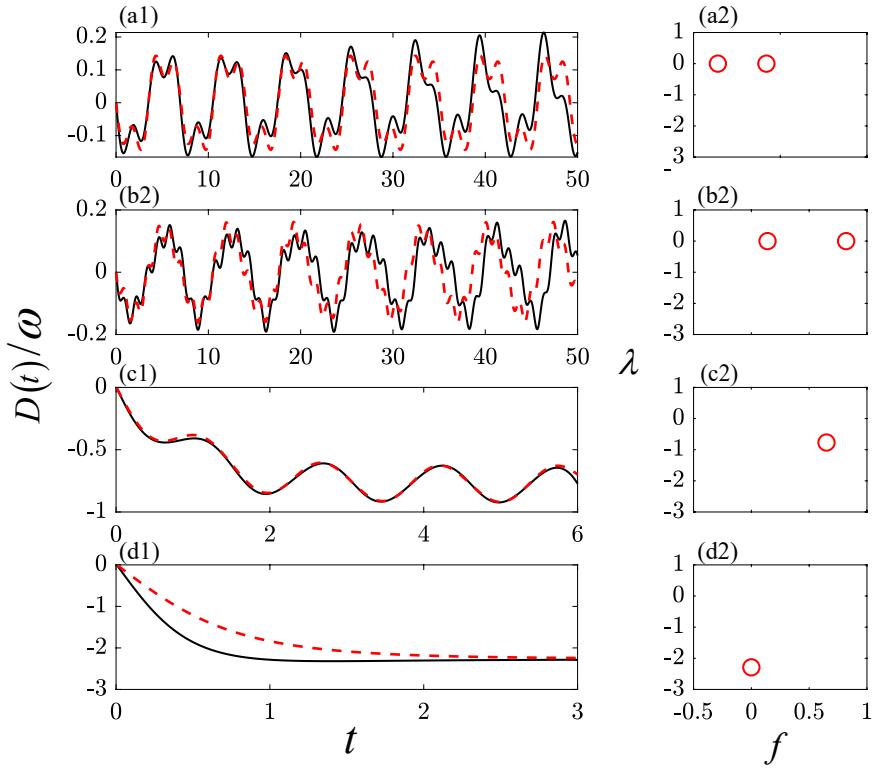
Figure 3: The plots of $D(t)$, given by Eq. (39), and their characteristics for the original ADM, given by Eq. (1) and effective Hamiltonian H_{eff} given by Eq. (4) in finite systems at the represented points indicated in Fig. 2. The plots in (a1)-(d1) are obtained by numerical simulations, the solid black line represents the numerical results obtained from the full ADM, whereas the red dashed line corresponds to the analytical result obtained from Eq. (36). The corresponding decay rates λ and frequencies f, plotted in (a2)-(d2), are extracted from the plots of $D(t)/\omega$. The number of atoms in the system is $N = 100$, and the bosonic Hilbert space is truncated at $n_{\text{max}} = 140$. Employing a larger bosonic cutoff n_{max} or increasing the number of atoms N does not alter the system's dynamical behavior over any finite time interval. These results are in accordance with the predictions from the analysis of the effective Hamiltonians. The time in the figure is in units of ω^{-1}

which is a measure of the revival for the initial state $|\psi(0)\rangle$. It allows us to characterize the properties of a system, provided that a proper initial state is chosen. We choose the empty state as the initial state $|\psi(0)\rangle = |\Downarrow\rangle |0\rangle$ and calculate its evolved state

$$|\psi(t)\rangle = \exp(-iHt)|\psi(0)\rangle, \tag{35}$$

where states $|\Downarrow\rangle$ and $|0\rangle$ are defined by $J_z|\Downarrow\rangle = -N/2|\Downarrow\rangle$ and $a|0\rangle = 0$, respectively. Before the computation for the finite ADM system, we would like to estimate the possible result.

We start with the investigation for the effective Hamiltonian H_{eff}, which can be dealt with analytically. The corresponding initial state becomes $|\psi(0)\rangle = |0\rangle_a |0\rangle_b$ and evolved state is $|\psi(t)\rangle = \exp(-iH_{\text{eff}}t)|\psi(0)\rangle$, correspondingly. Note that the initial state can also be written in the form $|\psi(0)\rangle = |0\rangle_{d_1} |0\rangle_{d_2}$, satisfying $d_1|\psi(0)\rangle = d_2|\psi(0)\rangle = 0$, which allows the product form of $L(t)$. In the thermodynamic limit, the Loschmidt echo has the following

approximate expressions in each regions

$$
L(t) \approx \begin{cases} \left[1 - 2A^2 \sin^2(\Omega_1 t)\right]\left[1 - 2B^2 \sin^2(\Omega_2 t)\right], & \text{NP} \\ \left[1 - 2A^2 \sin^2(\Omega_1 t)\right]\left[1 - 2B^2 \sin^2(\Omega_2 t)\right], & \text{SP}_1 \\ \left[1 - 2A^2 \sin^2(\Omega_1 t)\right]\left[\cosh(\Omega_2 t)\right]^{-1}, & \text{SP}_2 \\ \left[\cosh(\Omega_1 t)\right]^{-1}\left[\cosh(\Omega_2 t)\right]^{-1}, & \text{SP}_3 \end{cases}, \tag{36}
$$

where the parameters A and B are given explicitly as

$$
A = \frac{2}{1 + 2\tanh^{-2}\theta_1} = \frac{2(\omega + g_1 - \text{sgn}(\omega + g_1)\Omega_1)}{(\omega + g_1 - \Omega_1)^2 + 2g_2^2}, \tag{37}
$$

and

$$
B = \frac{2}{1 + 2\tanh^{-2}\theta_2} = \frac{2(\omega - g_1 - \text{sgn}(\omega - g_1)\Omega_1)}{(\omega - g_1 - \Omega_2)^2 + 2g_2^2}, \tag{38}
$$

respectively. The details of the calculation can be found in Appendix B. In each region, $L(t)$ is the product of two functions, which take different configurations. For the SP$_1$ region, it is the product of two periodic functions. For the SP$_2$ region, it is the product of a periodic function and a decaying function. For the SP$_3$ region, it is the product of two decaying functions. The reason why the product of the two functions adopts distinct configurations in different regions is that the underlying Hamiltonians are combined differently: whenever the effective Hamiltonian contains a harmonic or anti-harmonic oscillator, it supplies the periodic factor, whereas the presence of an inverted harmonic oscillator provides the decaying factor. We refer these phases to as hierarchic superradiant phases. It is noteworthy that the phase structure revealed by the Loschmidt echo exhibits considerable robustness with respect to the choice of initial states. We further investigate an intriguing special case where the system is initially prepared with all atoms in the excited state and the optical field in the vacuum state. Through a global SU(2) spin rotation transformation $J_z \rightarrow -J_z, J_\pm \rightarrow J_\mp$, the dynamical behavior under this initial condition can be rigorously mapped to the case with the ground state as the initial condition [41,67,68], which constitutes the main focus of this work. This symmetry operation leads to an important physical consequence: the effective phase diagram measured from this initial state becomes a mirror image of the phase diagram shown in Fig. 1(b) specifically manifesting as an exchange between the SP$_1$ and SP$_3$ regions, while the SP$_2$ region remains unchanged.

We note that the function $\left[\cosh(\Omega_i t)\right]^{-1} \approx 2e^{-\Omega_i t}$, decaying exponentially with rate Ω_i, after long time scale. Then, the oscillating frequency and the decay rate can be the dynamic characters of the hierarchic SPs. In order to characterize the hierarchy of the phases, we focus on the quantity

$$
D(t) = \frac{\partial}{\partial t} \ln L(t), \tag{39}
$$

because we have

$$
\frac{\partial}{\partial t} \ln e^{-\Omega_i t} = -\Omega_i. \tag{40}
$$

It is expected that $D(t)$ is the sum of two simple functions, which take different configurations in each region of superradiant phases. Therefore, the factors Ω_1 and Ω_2 can be extracted from the long-time behavior of $D(t)$. For the SP$_1$ region, $D(t)$ oscillates around zero, from which two frequencies $f_1 = \Omega_1/\pi$ and $f_2 = \Omega_2/\pi$ can be extracted. In the SP$_2$ region, it oscillates around a constant, from which the oscillating frequency f_1 and the balance point $-\Omega_2$ can be extracted. In the SP$_3$ region, it decays to a constant, from which the decay rate $\lambda = -(\Omega_1 + \Omega_2)$ can be extracted. What is shown in Fig. 2 is the analytical result of the decay rate

$$
\lambda = -(\Omega_1 + \Omega_2)/\omega, \tag{41}
$$

and the sum of frequencies

$$f = (f_1 + f_2)/\omega, \tag{42}$$

which can be extracted from the echo of the evolved state of the effective Hamiltonian H_{eff}. We can see the non-analytical behaviors of the plots at the phase boundaries.

Now, we turn to the computation of the corresponding quantities for the original ADM Hamiltonian. For a system with a finite number of atoms, the dimension of the Hilbert space is infinite. Therefore, the time evolution of the initial state is computed using exact diagonalization under the truncation approximation. The computations are performed using a uniform mesh in the time discretization for the truncated matrix. We selected four representative points in the four phases of the ADM to perform quench dynamics verification, and the results are shown in Fig. 3. Within the time scales of our numerical simulations, our results do not depend on the matrix size. The extracted decay rate λ and frequency f correspond to those in Fig. 2. The results are in accordance with the predictions from the analysis of the effective Hamiltonians. This demonstrates that there indeed exist hierarchical superradiant phases within the traditional superradiant phase of the ADM.

5   Summary

In summary, we have demonstrated that the conventional superradiant phase can be further separated into three regions. The underlying mechanism is the existence of the exceptional points in the effective Hamiltonians in the thermodynamic limit. Unlike traditional quantum phase transitions that typically occur in the ground state of the system, this constitutes a dynamical phase transition where the phase separations arise from sudden changes in the complete set of eigenstates. In this sense, the proposed phase diagram is not merely a mathematical concept, but definitely results in evident observations. Numerical simulations have been performed to compute the Loschmidt echo for finite systems. The results indicate that such observables are sufficient to characterize the hierarchical superradiant phases.

Acknowledgements

Funding information   This work was supported by the National Natural Science Foundation of China (under Grant No. 12374461).

A   Diagonalization of the Hamiltonians

In this appendix, we provide the derivation of the diagonalization of the Hamiltonian $\mathcal{H}$, which is equivalent to the two Hamiltonians H_1 and H_2 given in the main text. The Hamiltonian reads

$$\mathcal{H} = \mu \beta^\dagger \beta + \frac{\Delta}{2} \left(\beta^\dagger \beta^\dagger + \beta \beta \right), \tag{A1}$$

where β is the bosonic annihilation operator. Here, we do not restrict the range of μ and Δ, and $\mathcal{H}$ naturally satisfies

$$\begin{aligned} H_1 &= \mathcal{H}(\mu = \omega + g_1, \Delta = g_2), \\ H_2 &= \mathcal{H}(\mu = \omega - g_1, \Delta = g_2). \end{aligned} \tag{A2}$$

We assume that there exists a Bogoliubov transformation

$$\gamma = \sinh(\theta) \beta^\dagger + \cosh(\theta) \beta, \tag{A3}$$

that allows for the diagonalization of the Hamiltonian $\mathcal{H}$. Here, γ is also the bosonic annihilation operator and the inverse transformation is

$$\beta = \cosh(\theta)\gamma - \sinh(\theta)\gamma^{\dagger}. \tag{A4}$$

The coefficient θ is determined by the following process. Substituting the transformation into $\mathcal{H}$ we have

$$
\begin{aligned}
\mathcal{H} &= \frac{1}{2}[\Delta\cosh(2\theta) - \mu\sinh(2\theta)]\left[(\gamma^{\dagger})^2 + \gamma^2\right] \\
&+ \left[\mu\cosh^2(\theta) - \frac{\Delta}{2}\sinh(2\theta)\right]\gamma^{\dagger}\gamma \\
&+ \left[\mu\sinh^2(\theta) - \frac{\Delta}{2}\sinh(2\theta)\right]\left(1 + \gamma^{\dagger}\gamma\right).
\end{aligned} \tag{A5}
$$

We consider the following two cases respectively.

(i) $|\mu| > |\Delta|$, the Hamiltonian can be written as the diagonalized form

$$\mathcal{H} = \mathrm{sgn}(\mu)[\sqrt{\mu^2 - \Delta^2}\left(\gamma^{\dagger}\gamma + \frac{1}{2}\right)] - \frac{\mu}{2}, \tag{A6}$$

when we take

$$\tanh(\theta) = \frac{\mu - \mathrm{sgn}(\mu)\sqrt{\mu^2 - \Delta^2}}{\Delta}. \tag{A7}$$

(ii) $|\mu| < |\Delta|$, the Hamiltonian can be written as the anti-diagonalized form

$$\mathcal{H} = \mathrm{sgn}(\Delta)\frac{1}{2}\{\sqrt{\Delta^2 - \mu^2}[(\gamma^{\dagger})^2 + \gamma^2]\} - \frac{\mu}{2}, \tag{A8}$$

when we take

$$\tanh(\theta) = \frac{\Delta - \mathrm{sgn}(\Delta)\sqrt{\Delta^2 - \mu^2}}{\mu}. \tag{A9}$$

B Calculation of the Loschmidt echos

In this appendix, we present the derivations of the evolved states $|\psi(t)\rangle$, given in Eqs. (B.2) and (B.6), respectively, and the corresponding Loschmidt echo L_j, given in Eq. (B.7), respectively, for the initial state $|0\rangle_{d_j}$, which is the vacuum state of the operator d_j (where $j = 1, 2$). The driven Hamiltonians are H_{ho}, H_{aho}, and H_{iho}, given in Eqs. (14), (15) and (16), respectively.

The initial state $|0\rangle_{d_j}$ can be spanned by the common eigenstates $\{|l\rangle_j, l \in [0, \infty)\}$ of the Hamiltonians H_{ho}, H_{aho} and H_{iho}, in the form

$$|0\rangle_{d_j} = \sum_{l=0}^{\infty}\left[\tanh(\theta_j)\right]^l A_l |2l\rangle_j, \tag{B.1}$$

where $|l\rangle_j = \frac{1}{\sqrt{l!}}\left(\gamma_j^{\dagger}\right)^l |0\rangle_{\gamma_j}$ and $|0\rangle_{\gamma_j}$ is the vacuum state of the operator γ_j. The coefficients $\tanh\theta_j$ is defined in Eqs. (A7) and (A9), and given explicitly in the main text in Eqs. (22), (23), (28), (29), (32) and (33). A_l obey the iteration relation $A_{l+1}\sqrt{2l+2} = A_l\sqrt{2l+1}$, where A_0 is a constant determined by normalization. Hence, the evolved states $|\psi(t)\rangle_j$ for the Hamiltonians H_{ho} and H_{aho} can be directly obtained as

$$|\psi(t)\rangle_j = \begin{cases} \exp(-iH_{\mathrm{ho}}t)|0\rangle_{d_j} = \sum_{l=0}^{\infty}\exp(-i2l\Omega_j t)\left[\tanh(\theta_j)\right]^l A_l |2l\rangle_{d_j}, \\ \exp(-iH_{\mathrm{aho}}t)|0\rangle_{d_j} = \sum_{l=0}^{\infty}\exp(i2l\Omega_j t)\left[\tanh(\theta_j)\right]^l A_l |2l\rangle_{d_j}, \end{cases} \tag{B.2}$$

However, the set of states $\{|l\rangle_j\}$ are no longer the eigenstates of H_{iho}. We have to take another approach to derive the corresponding $|\psi(t)\rangle_j$. We note that the time evolution operator $U(t) = \exp(-iH_{\text{iho}}t)$ is nothing but the squeezing operator in quantum optics [56, 66]. This allows us to establish the relation

$$\mathcal{H}(t)U(t)|0\rangle_{\gamma_j} = \mathcal{H}(t)|\psi(t)\rangle_j = 0, \tag{B.3}$$

with

$$\mathcal{H}(t) = \gamma_j \cosh\left(\Omega_j t\right) + \gamma_j^\dagger i(-1)^{j+1}\sinh\left(\Omega_j t\right). \tag{B.4}$$

This indicates that the evolved state $|\psi(t)\rangle_j$ is the instantaneous zero-energy eigenstate of the auxiliary time-dependent Hamiltonian $\mathcal{H}(t)$. The evolved state can be obtained as

$$U(t)|0\rangle_{\gamma_j} = \sqrt{\text{sech}\left(\Omega_j t\right)} \sum_{l=0}^{\infty} \frac{\sqrt{(2l)!}}{l!2^l} \left[(-1)^j i \tanh(|\Omega_j| t)\right]^l |2l\rangle_{\gamma_j}, \tag{B.5}$$

by using the series method. If the initial state is the vacuum state $|0\rangle_{d_j}$ of the operator d_j, then the evolved state can be expressed as

$$|\psi(t)\rangle_j = \sum_{l=0}^{\infty} \frac{1}{\sqrt{2l!}} \mathcal{H}(t)^{2l} \left[\tanh(\theta_j)\right]^l A_l U(t)|0\rangle_{\gamma_j}. \tag{B.6}$$

Then the corresponding $L_j(t)$ are obtained as

$$L_j(t) \approx \begin{cases} \left|\langle 0|_{d_j} \exp\left(-iH_{\text{ho}}t\right)|0\rangle_{d_j}\right|^2 = 1 - \frac{8\tanh^2(\theta_j)}{\left[2+\tanh^2(\theta_j)\right]^2}\sin^2\left(\Omega_j t\right), \\ \left|\langle 0|_{d_j} \exp\left(-iH_{\text{iho}}t\right)|0\rangle_{d_j}\right|^2 = \left[\cosh\left(\Omega_j t\right)\right]^{-1}, \\ \left|\langle 0|_{d_j} \exp\left(-iH_{\text{aho}}t\right)|0\rangle_{d_j}\right|^2 = 1 - \frac{8\tanh^2(\theta_j)}{\left[2+\tanh^2(\theta_j)\right]^2}\sin^2\left(\Omega_j t\right), \end{cases} \tag{B.7}$$

This corresponds to Eqs. (36), (37), and (38) in the main text.

References

[1] K. Stranius, M. Hertzog and K. Börjesson, *Selective manipulation of electronically excited states through strong light–matter interactions*, Nature Communications **9**(1), 2273 (2018), doi:https://doi.org/10.1038/s41467-018-04736-1.

[2] J. Zhou, B. Huang, Z. Yan and J.-C. G. Bünzli, *Emerging role of machine learning in light-matter interaction*, Light: Science & Applications **8**(1), 84 (2019), doi:https://doi.org/10.1038/s41377-019-0192-4.

[3] N. S. Mueller, Y. Okamura, B. G. Vieira, S. Juergensen, H. Lange, E. B. Barros, F. Schulz and S. Reich, *Deep strong light–matter coupling in plasmonic nanoparticle crystals*, Nature **583**(7818), 780 (2020), doi:https://doi.org/10.1038/s41586-020-2508-1.

[4] N. Rivera and I. Kaminer, *Light–matter interactions with photonic quasiparticles*, Nature Reviews Physics **2**(10), 538 (2020), doi:https://doi.org/10.1038/s42254-020-0224-2.

[5] Z. Zhiqiang, C. H. Lee, R. Kumar, K. Arnold, S. J. Masson, A. Parkins and M. Barrett, *Nonequilibrium phase transition in a spin-1 Dicke model*, Optica **4**(4), 424 (2017), doi:https://doi.org/10.1364/OPTICA.4.000424.

[6] N. Marquez Peraca, X. Li, J. M. Moya, K. Hayashida, D. Kim, X. Ma, K. J. Neubauer, D. Fallas Padilla, C.-L. Huang, P. Dai *et al.*, *Quantum simulation of an extended Dicke model with a magnetic solid*, Communications Materials **5**(1), 42 (2024), doi:https://doi.org/10.1038/s43246-024-00479-3.

[7] A. T. Black, H. W. Chan and V. Vuletić, *Observation of collective friction forces due to spatial self-organization of atoms: From Rayleigh to Bragg scattering*, Physical Review Letters **91**(20), 203001 (2003), doi:https://doi.org/10.1103/PhysRevLett.91.203001.

[8] K. Baumann, C. Guerlin, F. Brennecke and T. Esslinger, *Dicke quantum phase transition with a superfluid gas in an optical cavity*, Nature **464**(7293), 1301 (2010), doi:https://doi.org/10.1038/nature09009.

[9] R. H. Dicke, *Coherence in spontaneous radiation processes*, Physical review **93**(1), 99 (1954), doi:https://doi.org/10.1103/PhysRev.93.99.

[10] N. Lambert, C. Emary and T. Brandes, *Entanglement and the phase transition in single-mode superradiance*, Physical Review Letters **92**(7), 073602 (2004), doi:https://doi.org/10.1103/PhysRevLett.92.073602.

[11] C. Emary and T. Brandes, *Chaos and the quantum phase transition in the Dicke model*, Physical Review E **67**(6), 066203 (2003), doi:https://doi.org/10.1103/PhysRevE.67.066203.

[12] K. Hepp and E. H. Lieb, *Equilibrium statistical mechanics of matter interacting with the quantized radiation field*, Physical Review A **8**(5), 2517 (1973), doi:https://doi.org/10.1103/PhysRevA.8.2517.

[13] Y. K. Wang and F. Hioe, *Phase transition in the Dicke model of superradiance*, Physical Review A **7**(3), 831 (1973), doi:https://doi.org/10.1103/PhysRevA.7.831.

[14] D. Ferraro, M. Campisi, G. M. Andolina, V. Pellegrini and M. Polini, *High-power collective charging of a solid-state quantum battery*, Physical Review Letters **120**(11), 117702 (2018), doi:https://doi.org/10.1103/PhysRevLett.120.117702.

[15] G. M. Andolina, M. Keck, A. Mari, V. Giovannetti and M. Polini, *Quantum versus classical many-body batteries*, Physical Review B **99**(20), 205437 (2019), doi:https://doi.org/10.1103/PhysRevB.99.205437.

[16] A. Crescente, M. Carrega, M. Sassetti and D. Ferraro, *Ultrafast charging in a two-photon Dicke quantum battery*, Physical Review B **102**(24), 245407 (2020), doi:https://doi.org/10.1103/PhysRevB.102.245407.

[17] F.-Q. Dou, Y.-Q. Lu, Y.-J. Wang and J.-A. Sun, *Extended Dicke quantum battery with interatomic interactions and driving field*, Physical Review B **105**(11), 115405 (2022), doi:https://doi.org/10.1103/PhysRevB.105.115405.

[18] J. Q. Quach, K. E. McGhee, L. Ganzer, D. M. Rouse, B. W. Lovett, E. M. Gauger, J. Keeling, G. Cerullo, D. G. Lidzey and T. Virgili, *Superabsorption in an organic microcavity: Toward a quantum battery*, Science Advances **8**(2), eabk3160 (2022), doi:https://doi.org/10.1126/sciadv.abk3160.

[19] D.-L. Yang, F.-M. Yang and F.-Q. Dou, *Three-level Dicke quantum battery*, Physical Review B **109**(23), 235432 (2024), doi:https://doi.org/10.1103/PhysRevB.109.235432.

[20] L. Wang, S.-Q. Liu, F.-l. Wu, H. Fan and S.-Y. Liu, *Deep strong charging in a multi-photon anisotropic Dicke quantum battery*, Physical Review A **110**(4), 042419 (2024), doi:https://doi.org/10.1103/PhysRevA.110.042419.

[21] C. Emary and T. Brandes, *Quantum chaos triggered by precursors of a quantum phase transition: the Dicke model*, Physical Review Letters **90**(4), 044101 (2003), doi:https://doi.org/10.1103/PhysRevLett.90.044101.

[22] P. Kirton, M. M. Roses, J. Keeling and E. G. Dalla Torre, *Introduction to the Dicke model: From equilibrium to nonequilibrium, and vice versa*, Advanced Quantum Technologies **2**(1-2), 1800043 (2019), doi:https://doi.org/10.1002/qute.201800043.

[23] B. M. Garraway, *The Dicke model in quantum optics: Dicke model revisited*, Philosophical Transactions of the Royal Society A: Mathematical, Physical and Engineering Sciences **369**(1939), 1137 (2011), doi:https://doi.org/10.1098/rsta.2010.0333.

[24] J. Vidal and S. Dusuel, *Finite-size scaling exponents in the Dicke model*, Europhysics Letters **74**(5), 817 (2006).

[25] M. Bhaseen, J. Mayoh, B. Simons and J. Keeling, *Dynamics of nonequilibrium Dicke models*, Physical Review A **85**(1), 013817 (2012), doi:https://doi.org/10.1103/PhysRevA.85.013817.

[26] E. M. Kessler, G. Giedke, A. Imamoglu, S. F. Yelin, M. D. Lukin and J. I. Cirac, *Dissipative phase transition in a central spin system*, Physical Review A **86**(1), 012116 (2012), doi:https://doi.org/10.1103/PhysRevA.86.012116.

[27] E. G. D. Torre, S. Diehl, M. D. Lukin, S. Sachdev and P. Strack, *Keldysh approach for nonequilibrium phase transitions in quantum optics: Beyond the Dicke model in optical cavities*, Physical Review A **87**(2), 023831 (2013), doi:https://doi.org/10.1103/PhysRevA.87.023831.

[28] M. Kloc, P. Stránský and P. Cejnar, *Quantum phases and entanglement properties of an extended Dicke model*, Annals of Physics **382**, 85 (2017), doi:https://doi.org/10.1016/j.aop.2017.04.005.

[29] M. Kloc, P. Stránský and P. Cejnar, *Monodromy in Dicke superradiance*, Journal of Physics A: Mathematical and Theoretical **50**(31), 315205 (2017), doi:https://doi.org/10.1088/1751-8121/aa7a95.

[30] P. Cejnar, P. Stránský, M. Macek and M. Kloc, *Excited-state quantum phase transitions*, Journal of Physics A: Mathematical and Theoretical **54**(13), 133001 (2021), doi:https://doi.org/10.1088/1751-8121/abdfe8.

[31] H. Carmichael, C. Gardiner and D. Walls, *Higher order corrections to the Dicke superradiant phase transition*, Physics Letters A **46**(1), 47 (1973), doi:https://doi.org/10.1016/0375-9601(73)90679-8.

[32] G. C. Duncan, *Effect of antiresonant atom-field interactions on phase transitions in the Dicke model*, Physical Review A **9**(1), 418 (1974), doi:https://doi.org/10.1103/PhysRevA.9.418.

[33] T. Kato, *Perturbation Theory for Linear Operators*, vol. 132, Springer Science & Business Media, doi:https://doi.org/10.1007/978-3-642-66282-9 (1995).

[34] M. V. Berry, *Physics of nonhermitian degeneracies*, Czechoslovak journal of physics **54**(10), 1039 (2004), doi:https://doi.org/10.1023/B:CJOP.0000044002.05657.04.

[35] W. D. Heiss, *The physics of exceptional points*, Journal of Physics A: Mathematical and Theoretical **45**(44), 444016 (2012), doi:https://doi.org/10.1088/1751-8113/45/44/444016.

[36] A. McDonald, T. Pereg-Barnea and A. Clerk, *Phase-dependent chiral transport and effective non-Hermitian dynamics in a bosonic Kitaev-Majorana chain*, Phys. Rev. X **8**(4), 041031 (2018), doi:https://doi.org/10.1103/PhysRevX.8.041031.

[37] Y.-X. Wang and A. Clerk, *Non-Hermitian dynamics without dissipation in quantum systems*, Phys. Rev. A **99**(6), 063834 (2019), doi:https://doi.org/10.1103/PhysRevA.99.063834.

[38] V. P. Flynn, E. Cobanera and L. Viola, *Deconstructing effective non-Hermitian dynamics in quadratic bosonic Hamiltonians*, New Journal of Physics **22**(8), 083004 (2020), doi:https://doi.org/10.1088/1367-2630/ab9e87.

[39] J. Del Pino, J. J. Slim and E. Verhagen, *Non-Hermitian chiral phononics through optomechanically induced squeezing*, Nature **606**(7912), 82 (2022), doi:https://doi.org/10.1038/s41586-022-04609-0.

[40] Y.-N. Wang, W.-L. You and G. Sun, *Quantum criticality in interacting bosonic Kitaev-Hubbard models*, Phys. Rev. A **106**(5), 053315 (2022), doi:https://doi.org/10.1103/PhysRevA.106.053315.

[41] T. Bilitewski and A. M. Rey, *Manipulating growth and propagation of correlations in dipolar multilayers: From pair production to bosonic Kitaev models*, Phys. Rev. L **131**(5), 053001 (2023), doi:https://doi.org/10.1103/PhysRevLett.131.053001.

[42] M. Ughrelidze, V. P. Flynn, E. Cobanera and L. Viola, *Interplay of finite-and infinite-size stability in quadratic bosonic lindbladians*, Phys. Rev. A **110**(3), 032207 (2024), doi:https://doi.org/10.1103/PhysRevA.110.032207.

[43] J. J. Slim, C. C. Wanjura, M. Brunelli, J. Del Pino, A. Nunnenkamp and E. Verhagen, *Optomechanical realization of the bosonic Kitaev chain*, Nature **627**(8005), 767 (2024), doi:https://doi.org/10.1038/s41586-024-07174-w.

[44] J. H. Busnaina, Z. Shi, A. McDonald, D. Dubyna, I. Nsanzineza, J. S. Hung, C. S. Chang, A. A. Clerk and C. M. Wilson, *Quantum simulation of the bosonic Kitaev chain*, Nature Communications **15**(1), 3065 (2024), doi:https://doi.org/10.1038/s41467-024-47186-8.

[45] J.-M. Hu, B. Wang and Z.-L. Xiang, *Bosonic holes in quadratic bosonic systems*, arXiv preprint arXiv:2408.01059 (2024), doi:https://doi.org/10.48550/arXiv.2408.01059.

[46] K. Zhou, B. Zeng and Y. Hu, *Non-Hermitian Aharonov-Bohm cage in bosonic Bogoliubov-de gennes systems*, Phys. Rev. B **111**, 224308 (2025), doi:10.1103/y174-pms8.

[47] R. Wang and X. Z. Zhang, *Probing quantum phase transitions in a staggered bosonic Kitaev chain via fock space resolved localization-delocalization transitions*, Phys. Rev. B **112**, 125117 (2025), doi:10.1103/6lhp-8q6k.

[48] D. K. He and Z. Song, *Hidden exceptional point and the localization-delocalization phase transition in the Hermitian bosonic Kitaev model*, Physical Review B **111**(3), 035131 (2025), doi:https://doi.org/10.1103/PhysRevB.111.035131.

[49] D. K. He and Z. Song, *Higher order coherence as witness of exceptional point in Hermitian bosonic Kitaev dimer*, New Journal of Physics **27**(9), 094504 (2025), doi:10.1088/1367-2630/ae014f.

[50] W. Buijsman, V. Gritsev and R. Sprik, *Nonergodicity in the anisotropic Dicke model*, Physical Review Letters **118**(8), 080601 (2017), doi:https://doi.org/10.1103/PhysRevLett.118.080601.

[51] P. Das, D. S. Bhakuni and A. Sharma, *Phase transitions of the anisotropic Dicke model*, Physical Review A **107**(4), 043706 (2023), doi:https://doi.org/10.1103/PhysRevA.107.043706.

[52] X. Zhu, J.-H. Lü, W. Ning, L.-T. Shen, F. Wu and Z.-B. Yang, *Quantum geometric tensor and critical metrology in the anisotropic Dicke model*, Physical Review A **109**(5), 052621 (2024), doi:https://doi.org/10.1103/PhysRevA.109.052621.

[53] G. Vivek, D. Mondal, S. Chakraborty and S. Sinha, *Self-trapping phenomenon, multistability and chaos in open anisotropic Dicke dimer*, Physical Review Letters **134**(11), 113404 (2025), doi:https://doi.org/10.1103/PhysRevLett.134.113404.

[54] P. Das, D. S. Bhakuni, L. F. Santos and A. Sharma, *Periodically and quasiperiodically driven anisotropic Dicke model*, Physical Review A **108**(6), 063716 (2023), doi:https://doi.org/10.1103/PhysRevA.108.063716.

[55] X.-Y. Chen, Y.-Y. Zhang, Q.-H. Chen and H.-Q. Lin, *Phase transitions in the anisotropic Dicke-stark model with a^2 terms*, Physical Review A **110**(6), 063722 (2024), doi:https://doi.org/10.1103/PhysRevA.110.063722.

[56] V. Subramanyan, S. S. Hegde, S. Vishveshwara and B. Bradlyn, *Physics of the inverted harmonic oscillator: From the lowest Landau level to event horizons*, Annals of Physics **435**, 168470 (2021), doi:https://doi.org/10.1016/j.aop.2021.168470.

[57] G. Barton, *Quantum mechanics of the inverted oscillator potential*, Annals of Physics **166**(2), 322 (1986).

[58] K. Gietka and T. Busch, *Inverted harmonic oscillator dynamics of the nonequilibrium phase transition in the Dicke model*, Physical Review E **104**(3), 034132 (2021), doi:https://doi.org/10.1103/PhysRevE.104.034132.

[59] A. I. Lvovsky and M. G. Raymer, *Continuous-variable optical quantum-state tomography*, Reviews of modern physics **81**(1), 299 (2009), doi:https://doi.org/10.1103/RevModPhys.81.299.

[60] M. Cramer, M. B. Plenio, S. T. Flammia, R. Somma, D. Gross, S. D. Bartlett, O. Landon-Cardinal, D. Poulin and Y.-K. Liu, *Efficient quantum state tomography*, Nature Communications **1**(1), 149 (2010), doi:https://doi.org/10.1038/ncomms1147.

[61] M. Christandl and R. Renner, *Reliable quantum state tomography*, Physical Review Letters **109**(12), 120403 (2012), doi:https://doi.org/10.1103/PhysRevLett.109.120403.

[62] A. Vukics and P. Domokos, *Adequacy of the Dicke model in cavity QED: A counter-no-go statement*, Physical Review A **86**(5), 053807 (2012).

[63] P. Nataf and C. Ciuti, *No-go theorem for superradiant quantum phase transitions in cavity QED and counter-example in circuit QED*, Nature Communications **1**(1), 72 (2010).

[64] T. Ye, Y.-Z. Wang, X.-Y. Chen, Q.-H. Chen and H.-Q. Lin, *Superradiant phase transitions in the quantum Rabi model: Overcoming the no-go theorem through anisotropy*, Physical Review A **111**(4), 043716 (2025).

[65] J. Vidal, S. Dusuel and T. Barthel, *Entanglement entropy in collective models*, Journal of Statistical Mechanics: Theory and Experiment **2007**(01), P01015 (2007).

[66] M. O. Scully and M. S. Zubairy, *Quantum Optics*, Cambridge university press (1997).

[67] A. Duha and T. Bilitewski, *Two-mode squeezing in Floquet-engineered power-law interacting spin models*, Physical Review A **109**(6), L061304 (2024).

[68] A. Duha, S. E. Begg and T. Bilitewski, *Nonequilibrium critical scaling of a squeezing phase transition*, Physical Review Letters **135**(15), 150401 (2025).